MEAN FLUXES AND BRIGHTNESS FIELDS IN STATISTICALLY HOMOGENEOUS BROKEN CLOUDS

D.A. Zimin and G.A. Titov

Institute of Atmospheric Optics,
Siberian Branch of the Russian Academy of Sciences, Tomsk
Received December 29, 1993

In this paper we present a study of the sensitivity of solar radiation statistical characteristics, due to modulation by statistically homogeneous cumulus clouds, to variations in the geometric shapes of cloud bottoms. It is shown that the mean fluxes and brightness fields, as calculated using four different cloud models (with the same probability of the Sun shadowing by a cloud), only weakly depend on the shape of individual cloud bottoms.

INTRODUCTION

In statistical describing of radiation transfer through clouds the problem of the construction of an optical model of cloud fields with random geometry (broken cloudiness) is a prime consideration. Simplest models approximate individual clouds by elementary geometrical bodies (such as cylinders, truncated paraboloids, spheres, etc). To simulate clouds realistically, more complex models are elaborated, that are based on the sum of random Gaussian fields,[1] as well as the construction of clouds with a prescribed fractal dimension which is inferred from satellite data[4–6] using n–step cascade processes,[2,3] and so on. However, numerical construction of such model cloud fields is highly laborious and demands very large amount of computing resources. At the same time, the experimental data on vertical geometrical structure of clouds are yet insufficient to construct adequately the statistically inhomogeneous models of broken cloudiness. Therefore, in practice the problems are solved under assumption of the statistical homogeneity of cloud fields.

At present there exist a number of mathematical models of statistically homogeneous broken cloudiness, in which clouds are approximated by cylinders of the same height, but of different base shape. Such an uncertainty brings up the question: How high is the sensitivity of mean fluxes and brightness fields of the statistically homogeneous cloud fields to variations of base shapes of individual clouds? Below we try to answer this question comparing mean radiant fluxes and brightness fields obtained in four models of statistically homogeneous broken cloudiness.

MODELS OF STATISTICALLY HOMOGENEOUS CLOUD FIELDS

Cloudiness is specified within the layer Λ: $0 \le z \le H$ as random scalar fields of extinction coefficient $\sigma k(\mathbf{r})$, single scattering albedo $\lambda k(\mathbf{r})$, and scattering phase function $g(\omega, \omega') k(\mathbf{r})$; here ω is the unit vector and $k(\mathbf{r})$ is the random indicator field

$$k(\mathbf{r}) = \begin{cases} 1, & \mathbf{r} \in G, \\ 0, & \mathbf{r} \notin G, \end{cases}$$

where G is the random set of points in Λ, where cloud occurs.

All cloud models discussed below treat clouds as H–height cylinders with various base shapes. The input parameters of models are the cloud amount index N and the mean (or some effective) horizontal size (diameter) $\overline{D}$.

Spatial distribution of dynamically noninteracting cumulus clouds, which forms horizontally homogeneous cloud field, can be considered as the Poisson distribution. Such an assumption is in good agreement with radar measurements[7] and allows one to relate simply model parameters to experimentally determined characteristics of cloudiness. We choose in the plane $z = 0$ m points according to the Poisson law $P(m) = (\overline{m})^m / m! \exp(-\overline{m})$ and distribute them uniformly into the circle of radius R, where $\overline{m} = vS$ is the mean number of points falling on the area $S = \pi R^2$. Value of R may always be taken sufficiently large, thus in solving practical problems the finite size of the area, in which cloud field is modeled, can be neglected. So obtained spatial Poisson flux of points $\mathbf{r}_1, \dots, \mathbf{r}_m$ fixes the cloud bottom geometric centers. The indicator function $k(\mathbf{r})$ is defined as

$$k(\mathbf{r}) = \bigcup_{i=1}^{m} q(\mathbf{r} - \mathbf{r}_i), q(\mathbf{r} - \mathbf{r}_i) = \begin{cases} 1, & \mathbf{r} \in A_i, \\ 0, & \mathbf{r} \notin A_i, \end{cases}$$

where A_i is the set of points possessed to the convex geometrical figure Γ centered on $\mathbf{r}_i$ which approximates an individual cloud; and q is the indicator function for the A_i set. Let us consider two models based on the Poisson point fluxes.

Model 1. Cloudiness is modeled using random mosaics[8] which are the set of convex, bounded polygons covering the space without overlapping.

The random mosaics are generated by the spatial Poisson flux of points $\mathbf{r}_1, \dots, \mathbf{r}_m$ according to the following rule: the cell C_i contains all spatial points closest to $\mathbf{r}_i$ (compared to the other points $\mathbf{r}_j$, $i \neq j$). So C_i will almost surely convex polygon because it is formed by several intersecting straight lines. We use the equivalent diameter D^{eq}, that is the diameter of a circle whose area is equal to the mean area of a random mosaic, as a

characteristic horizontal size of a mosaic. Mean number of cloud centers v per unit area is $\pi R^2 = v\pi(D^{eq})^2/4$. Value of indicator function $k(\mathbf{r})$ is determined for each cell independently. H—height cylinder with random mosaic C_i as a base is a cloud with probability N or cloudless gap with probability $1 - N$.

Model 2. Clouds are approximated by cylinders with circle of diameter D as a base, and centers distributed on one plane in accordance with the Poisson law with the mean density

$$v = -4 \ln(1 - N) / \pi D^2.$$

The probability of covering the viewing direction by clouds (value used throughout the paper) is defined as[9]

$$N_2(\theta) = 1 - \exp\left[-v\left(\pi\frac{D^2}{4} + D H \tan(\theta)\right)\right]. \tag{1}$$

Sampling cloud fields of the above—mentioned models, constructed based on the Poisson points ensembles in space, are shown in Figs. 1 and 2.
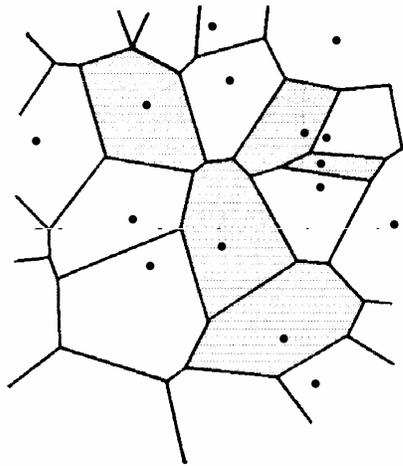
FIG. 1.   Random mosaics: points are the cell centers, clouds are shown by hatched random polygons.
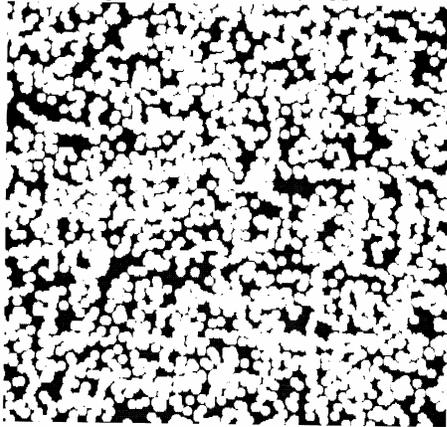
FIG. 2.   A sampling cloud field constructed on spatial Poisson point flux in region 25 by 25 km for $D = 0.5$ km.

As was already noted, cloud fields of models 1 and 2 are constructed in finite cylindrical region which is required to be large enough to reduce the number of escaping photons and thereby the computational error. However, if the region under simulation has too large horizontal size, the numerical construction of cloud field and photon trajectory simulation become tedious. There is not a general rule for determination of the optimal size of this region and usually this optimal size is found empirically. Based on numerous computations, in Ref. 10 it is proposed to take R values from $2H$ to $3H$.

Model 3 is constructed on the Poisson points fluxes on straight lines. The indicator field $k(\mathbf{r})$ is specified in the plane $z = 0$ within the rectangle $[0, X]\times[0, Y]$ as follows.

1. Stationary Poisson points fluxes are constructed on the coordinate axes independently with the correlation functions $B(x) = \exp(-A_x x)$ and $B(y) = \exp(-A_y y)$, where A_x and A_y are the mean number of points per unit length.

2. Independent values of $k(\mathbf{r})$ are assigned for each rectangle $[x_{j-1}, x_j] \times [y_{i-1}, y_i]$ according to the distribution function $N\delta(k(\mathbf{r}) - 1) + (1 - N)\delta(k(\mathbf{r}))$.

The field so obtained is statistically homogeneous, nonisotropic, with the exponential correlation function $B(x)B(y)$. Individual clouds in this model are parallelepipeds which can combine forming more complex structures. Reliable experimental data on variations of the cloud size along different directions are lacking; hence we assume that $A_x = A_y = A$ and cloud bottom is a square on the average. The parameter A is approximated as $A = [1.65(N - 0.5)^2 + 1.04]/\overline{D}$ (Ref. 11), here $\overline{D}$ is the mean horizontal cloud size. The probability of covering the viewing direction by clouds is defined as[10]

$$N_3(\theta) = 1 - (1 - N)\exp(-A N H \tan(\theta)). \tag{2}$$

A random cloud field is given in Fig. 3.
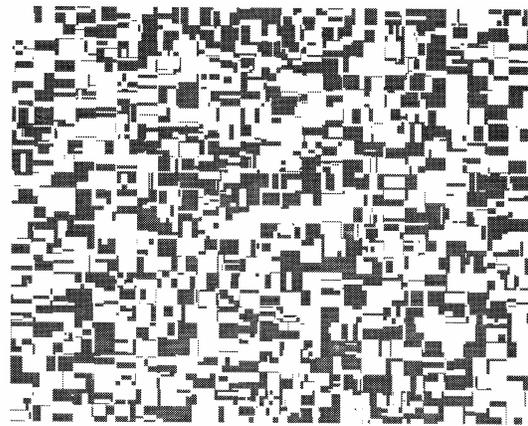
FIG. 3.   An example of random cloud field generated by Poisson points flux on the coordinate axes (region 25 by 25 km).

Model 4. Cloudiness is simulated with Gaussian random field. For the model description see Ref. 12. In statistically homogeneous case, the cloudiness is constructed as follows: the cylindrical cloud bases are formed by intersection of the

surface $w(x, y) = \max(\,|v(x, y) - c\,|,\ 0)$ and the plane $z = 0$, where $v(x, y)$ is the homogeneous Gaussian field with zero mean, the correlation function $K(x, y)$, and the variance $\sigma = K(0, 0)$. The indicator field is defined as

$$k(\mathbf{r}) = k(x,\ y,\ z) = \begin{cases} 1, & w(x, y) \geq 0, \\ 0, & w(x, y) < 0. \end{cases}$$

Following Ref. 12, we calculated with the correlation function

$$K(x, y) = \sigma^2\, J_0(\rho(x^2 + y^2))\,, \tag{3}$$

where J is the Bessel function, ρ is the radially spectral measure related to the correlation radius r as $J_0(\rho r) = 1/\sigma^2 e$, and the Gaussian field was approximately simulated according to formula[12]

$$v(x, y) \approx \frac{\sigma}{\sqrt{I}}\ \sum_{i=1}^{I} \sqrt{-\,2\,\ln(\alpha_i)}\ \cos((x\rho\cos\omega_i + y\,\rho\,\sin\omega_i) + 2\pi\,\beta_i). \tag{4}$$

Cloud parameters N and $\overline{D}$ are related to the input parameters of the model by formulas

$$\overline{D}^2 = 8\sqrt{2\pi}\,(N\,/\,\rho^2)\,d_2\exp(d_2\,/\,2);\ N = 2(1 - \Phi(d_2)). \tag{5}$$

The variance σ and the level of section c enter into Eq. (5) as the ratio $d_2 = c/\sigma$, therefore, one of them, for example, σ, can be fixed. (Hereinafter we set $\sigma = 0.5$.) Figure 4 gives a cloud field of this model.
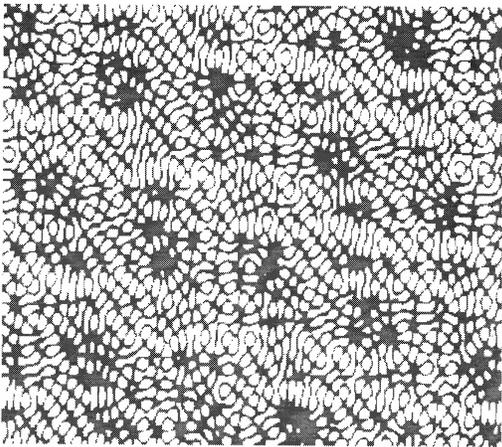
FIG. 4. *A sampling cloud field in the model based on the Gaussian random field (region* 25 *by* 25 *km).*

Reconciling the parameters. To estimate the influence of cloud bottom shape on the mean fluxes and brightness fields of visible solar radiation, the models should be reconciled upon the input parameters. Because we are interested in cloud–radiation interaction, reconciling should be performed so, that the cloud field characteristics exerting primary effect on radiation transfer to be close. It is therefore desirable to fit models parameters so that the mean fluxes of nonscattered radiation $<S>$ come coincident. This condition is necessary but not sufficient for the

coincidence of the mean diffuse fluxes. In this case, however, the agreement is expected in the mean diffuse transmission $<Q_s>$ and the mean albedo $<A>$. Clouds are optically thick and for small and intermediate cloud amount index the nonscattered radiation passes mostly through cloud gaps. For this reason, $<S>$ is governed primarily by the probability of covering the direction to sun by cloud $N(\xi_\otimes)$, there $\xi_\otimes$ is the solar zenith angle. Therefore, it seems naturally to require the equality of those probabilities for all the models.

In models 1 and 4, the above probabilities are unavailable in an analytical form. However, recognizing that for large optical thicknesses $<S> \cong N(\xi_\otimes)$, we propose the following reconciling procedure.

1. The mean fluxes calculated using model 4 are taken as reference ones.

2. Using analytical expression for the mean intensity of nonscattered radiation (see Ref. 11, Eq. (11)), the effective value of cloud diameter in model 3 is taken so that $<S_3> = <S_4>$, hereafter the subscript indicates the model number.

3. The effective diameter D_2^{eff} in the model 2 is taken to satisfy the condition $N_2(\xi_\otimes) = N_3(\xi_\otimes)$. From Eqs. (1) and (2) it follows that

$$D_2^{\mathrm{eff}} = -\,4\,\ln(1 - N)\,/\,(\pi\,N\,A). \tag{6}$$

4. The models 1 and 2 are reconciled, to the first approximation, by equating of cloud base areas in the models, that is equivalent to requirement that $D_1^{\mathrm{eff}} = D_2^{\mathrm{eff}}$.

At $\xi_\otimes = 0°$ and $N(0) = N$ the mean flux of nonscattered radiation is independent on the cloud horizontal size. For such a case, the effective cloud size in the model 3 is not uniquely determined, and D_3^{eff} is adjusted so as to bring the mean fluxes of scattered radiation in a closest agreement. Equation (6) relating cloud size in models 1 and 2 remains in force as it is devoid of the $\xi_{\mathring{A}}$ dependence. The dependence of the effective diameters in models 1, 2, and 3, obtained with the described procedure, on the cloud amount index and solar zenith angle is illustrated in Fig. 5. There and in the following figures, numbers are correspond to the models numbers. It is seen from the figure, that the effective horizontal cloud size is maximum in the model 4. In the models 1, 2, and 3 D^{eff} decreases significantly with increasing cloud amount index, being a nonmonotonic function of solar zenith angle.
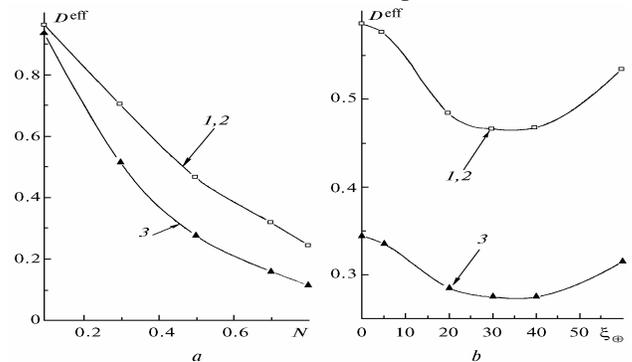
FIG. 5. *Reconciled effective cloud diameters in the models 1, 2, and 3 as a function of cloud amount index (a) and solar zenith angle (b) for* $\overline{D}_4 = 1$ *km.*

Calculational results.   In the context of model 3, the radiation transfer equation for mean radiant intensity was solved by Monte Carlo method. For other models we used technique for simulating the cloud and radiation fields.[13] Computations were performed with zero albedo of underlying surface and with scattering phase function corresponding to C_1 cloud model[14] and wavelength of 0.69 μm. Molecular and aerosol scattering was not considered. Optical and geometrical cloud characteristics were ranging within $0 \leq N \leq 0.9$, $0 \leq \xi_\otimes \leq 60°$, and $10 \leq \sigma \leq 60$ km^{-1}. The relative error in the mean fluxes did not exceed 1% throughout the computation.

We compared models, taking

$$\delta(F_i, F_j) = \left| \frac{F_i - F_j}{F_j} \right| \times 100\%, \quad F = <S>, <Q_s>, <A>$$

as a measure of "agreement" between the mean fluxes, and, in addition, the quantity

$$\delta(F_i) = \left| \frac{F_i - F_4}{F_4} \right| \times 100\%, \quad i = 1, 2, 3$$

as a characteristic of deviation from reference Gaussian model.

Figures 6 and 7 present dependence of the mean fluxes of direct, scattered transmitted, and reflected radiation on cloud amount index and solar zenith angle. For $N < 0.5$, the mean fluxes of nonscattered radiation agree within the computational accuracy (Fig. 6*a*), and the suspicion that $<S>$ is primarily determined by $N(\xi_\otimes)$ is well confirmed. For larger N, the contribution to $<S>$ from cloud–transmitted radiation becomes stronger. The models have different total areas of the optically thin cloud edges, that produces small (in absolute value) deviations in $<S_2>$ and $<S_3>$, however, because of their smallness, the $\delta(S_2)$ and $\delta(S_3)$ values can amount to 5–10%. The large $\delta(S_1)$ values at $N > 0.5$ and $10 < \xi_\otimes < 45°$ indicates that the use of the condition $D_1^{eq} = D_2^{eff}$ for reconciling in the given range of the parameters variation does not assure $N_1(\xi_\otimes) = N_2(\xi_\otimes)$.
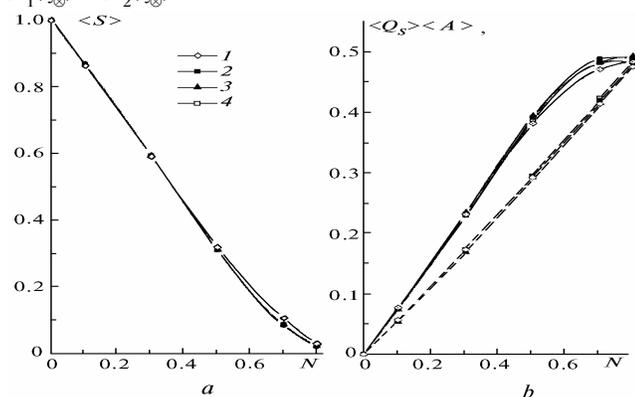
FIG. 6.   *Dependence of the mean radiant fluxes on cloud amount index at* $\sigma = 30$ km^{-1}, $\xi_\otimes = 10°$: $<S>$ *(a) and* $<Q_s>$ *(solid lines),* $<A>$ *(dashed lines) (b).*
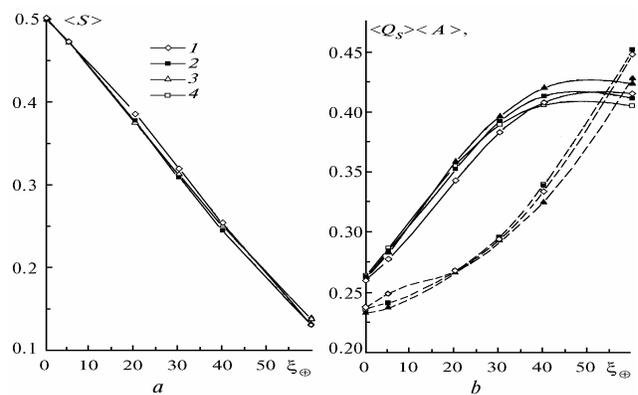
FIG. 7.   *Mean fluxes of solar radiation versus zenith angle at* $N = 0.5$ *and* $\sigma = 30$ km^{-1}: $<S>$ *(a) and* $<Q_s>$ *(solid lines),* $<A>$ *(dashed lines) (b).*

The reflected fluxes $<A_2>$ and $<A_4>$ agree to within the computational error over the entire range of the parameters variation (Figs. 6*b* and 7*b*). Also, the model 1 produces albedo value close to the above–mentioned ones, if the model is well–reconciled upon $<S>$, $\delta(<A_1>)$ is below 2%. Spread in $<Q_s>$ values of the models 1, 2, and 4 is primarily due to the mismatching between the direct radiation fluxes and is in complete agreement with the $<S>$ mismatching. For $\xi_\otimes > 30°$, the flux $<Q_{S3}>$ is somewhat greater, while the albedo $<A_3>$ is smaller, than their counterparts in the models, and increasing the solar zenith angle causes increase of $\delta(<Q_{S3}>)$ and $\delta(<A_3>)$ up to 5% at $\xi_\otimes = 60°$. Such a behavior of the fluxes is because the model 3 contains grater number of small clouds (Fig. 5), therefore, the role of cloud sides in the radiation transfer will be more important. In particular, since phase scattering function is strongly forward peaked, radiation leaving cloud sides contributes mainly to the transmission; and for constant $<S>$ the fraction of reflected radiation is thus reduced.

The growth of the extinction coefficient from 10 to 60 km^{-1} has little effect on the mean flux deviations. The nonscattered radiation fluxes in the models 2 and 3 reconciled by equating the probabilities of observing cloud along the line of sight to the Sun, show increasing agreement as the extinction coefficient increases, reaching almost complete coincidens for $\sigma > 30$ km^{-1}; moreover, even at $\sigma = 10$ km^{-1} the discrepancy does not exceed 2% (Fig. 8). Therefore, for σ varying between the above limits, equating the $N(\xi_\otimes)$ values can be considered as sufficient condition for reconciling upon the direct radiation. Due to the comparison procedure adopted, $\delta(<S_3>) = 0$. Albedo values in all models agree to within the computational error; the mean fluxes of scattered radiation are also close, $\delta(<Q_s>) \cong 1.5$–2%.
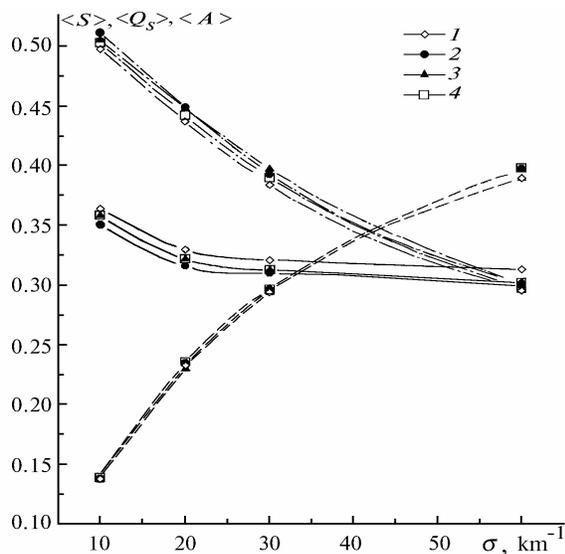
FIG. 8. Influence of the extinction coefficient σ on the mean radiant fluxes at N=0.5 and $\xi_\otimes$=30°: $<S>$ − solid, $<Q_s>$ − dot−dash, and $<A>$ − dashed lines.

The $\delta(S_1)$ value is 2−2.5% and weakly depends on σ, because the dominating cause for discrepancy of the models 1 and 2 is the insufficiently adjusted probabilities of covering

direction to Sun by clouds. To obtain the correct condition for reconciling is not the purpose of the paper; it is however hoped that fluxes of the model 1 can agree better with the other models if the nonscattered radiation is somehow brought in a closer agreement. One way is to use the above described comparison procedure, taking the model 1 as a reference one and adjusting the mean diameter in the model 3 according to $<S_1> = <S_3>$. Mean fluxes from the models 1, 2, and 3 so reconciled and computed at values of N and $\xi_\otimes$ which under the condition $D_1^{eff} = D_2^{eff}$ yield maximum differences in $<S_1>$ and $<S_3>$ are given in Table I. From the table it is seen that, as expected, the relative deviations of fluxes are within the computational error.

TABLE I.

$\xi_\otimes$	N	Model	$<Q_s>$	$<S>$	$<A>$	$<Q>$
20°	0.5	1	0.389	0.342	0.269	0.731
		2	0.389	0.344	0.267	0.733
		3	0.388	0.343	0.269	0.731
	0.7	1	0.207	0.411	0.382	0.618
		2	0.207	0.412	0.381	0.619
		3	0.207	0.410	0.383	0.617
30°	0.5	1	0.332	0.374	0.294	0.706
		2	0.332	0.376	0.292	0.708
		3	0.329	0.375	0.296	0.704
	0.7	1	0.165	0.428	0.407	0.593
		2	0.165	0.427	0.408	0.592
		3	0.164	0.426	0.410	0.590
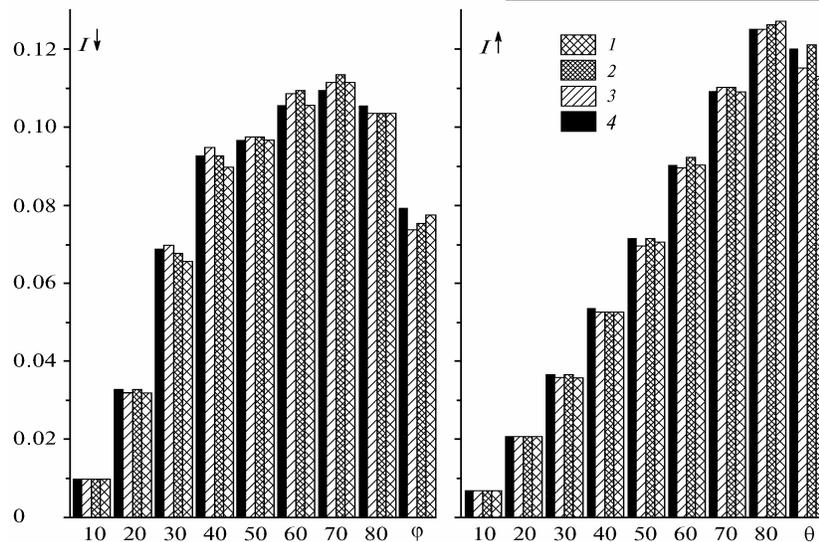
FIG. 9. Angular distributions of the mean intensity of reflected and transmitted radiation at $N = 0.5$, $\xi_\otimes = 30°$, and $\sigma = 30$ km^{-1}.

Coinciding mean fluxes can have different angular structure. To estimate the differences, we present histograms of angular distributions of scattered radiation (Fig. 9) defined as

$$I_i^{\uparrow(\downarrow)} = \int\limits_0^{2\pi} d\,\varphi \int\limits_{\theta_i}^{\theta_{i+1}} < I^{\uparrow(\downarrow)}(\theta,\,\varphi)> d\theta ,$$

$$0 \le \theta \le \frac{\pi}{2} , \quad \theta_{i+1} - \theta_i = 0.1 ,$$

where $< I^{\uparrow(\downarrow)}(\theta,\,\varphi)>$ is the mean intensity of transmitted (↓) and reflected (↑) radiation, respectively; θ and φ are the zenith and azimuth angles. It is seen that for the considered models the angular distributions agree well. Some differences in $I_i^{\uparrow(\downarrow)}$ are for the same reasons as the mean flux deviation. Computations have shown that, within the above−mentioned range of cloud amount index and solar zenith angle variations, the angular distributions qualitatively agree; $\delta(I)$ averages 5% that can be related to computational error not exceeding 4%.

CONCLUSION

The models examined generate quite different individual clouds and cloud field (Figs. 1–4). Nevertheless, on a proper reconciling input parameters, the externally unlike models are practically equivalent from the radiation transfer standpoint. An effective reconciling follows by equating probability of covering the viewing direction to Sun by clouds.

Thus, if experimentally determined values of $N(\xi_{\otimes})$ are used as an input parameter, radiative characteristics will be insensitive to the choice of a statistically homogeneous cloud model. This means, that assuming statistical homogeneity of cloud field allows computation of the mean radiant fluxes and brightness fields without accounting for cloud bottom shapes; therefore, in practice the most efficient and computer time saving cloud model can be chose.

REFERENCES

1. E.A. Babich and G.A. Titov, Atmos. Oceanic Opt. **5**, No. 7, 478–484 (1992).
2. B.B. Mandelbrot, Fluid Mech. **62**, 331–358 (1974).
3. D. Schertser and S. Lovejoy, in: *Fractals: the Physical Origin and Consequences* (Plenum Press, 1990), pp. 49–79.
4. S. Lovejov, Science **216**, 185–187 (1982).
5. F.S. Rhis and A. Waldvogel, Phys. Rev. Lett. **56**, No. 7, 764–787 (1986).
6. R.F. Calhan and J.H. Joseph, Monthly Weather Review **117**, 261–272 (1989).
7. Cho Han–Ru, J. Atmos. Sci. **35**, No. 1, 125 (1978).
8. L. Santalo, *Integral Geometry and Geometrical Probabilities* (Nauka, Moscow, 1983), 358 pp.
9. O.A. Avaste, Yu.R. Mullamaa, Kh.Yu. Niilisk, and M.A. Sulev, in: *Heat Exchange in Atmosphere* (Nauka, Moscow, 1972), pp. 134–139.
10. G.A. Titov, "*Statistical description of radiation transfer in clouds,*" Doctorate's Dissertation in Physical–Mathematical Sciences, Institute of Atmospheric Optics, Siberian Branch of the Academy of Sciences of the USSR, Tomsk (1988), 361 pp.
11. G.A. Titov, Opt. Atm. **1**, No. 4, 3–18 (1988).
12. B.A. Kargin and S.M. Prigarin, "*Simulation of stochastic fields of cumulus clouds and investigation of their radiative propertives by the Monte Carlo method,*" Preprint No. 817, Computing Center, Siberian Branch of the Academy of Sciences of the USSR, Novosibirsk (1988), 18 pp.
13. G.A. Titov, J. Atmos. Sci. **47**, No. 1, 24–37 (1990).
14. D. Deirmendjian, *Electromagnetic Scattering on Spherical Polydispersions* (American Elsevier, N.Y., 1969).